Journal of the Korean Nuclear Society
Volume 29, Number 1, pp. 35~44, February 1997

An Empirical Correlation for Critical Flow Rates of Subcooled Water Through Short Pipes with Small Diameters

Choon-Kyung Park, Jee-Won Park, and Moon-Ki Chung
Korea Atomic Energy Research Institute
Thermal Hydraulics Department
150 Dukjin-dong, Yusong-gu, Taejon 305-353, Korea

Moon-Hyun Chun
Korea Advanced Institute of Science and Technology
Department of Nuclear Engineering
373-1 Kusong-dong, Yusong-gu, Taejon 305-701, Korea

(Received May 11, 1996)

Abstract

Critical two-phase flow rates of subcooled water through short pipes ($L \leq 400$ mm) with small diameters ($D \leq 7.15$ mm) have been experimentally investigated for wide ranges of subcooling (0~199 ℃) and pressure (0.5~2.0 MPa). To examine the effects of various parameters (i.e., the location of flashing inception, the degree of subcooling, the stagnation temperature and pressure, and the pipe size) on the critical two-phase flow rates of subcooled water through short pipes with small diameters, a total of 135 runs were made for various combinations of test parameters using four different L/D test sections. Experimental results that show effects of various parameters on subcooled critical two-phase flow rates are presented in the form of graphs such as the dimensionless mass flux (G^*) versus the dimensionless subcooling (T^*_{sub}) curve. An empirical correlation expressed in terms of a dimensionless subcooling is also obtained for subcooled two-phase flow rates through present test sections. Comparisons between the mass fluxes calculated by present correlation and a total of 755 selected experimental data points of 9 different investigators show that the agreement is fairly good except for very low subcooling data obtained from small L/D (less than 10) orifices.

1. Introduction

The critical flow phenomenon has been studied extensively in both single-phase and two-phase systems because of its important role in the loss of coolant accident (LOCA) analyses of light water reactors and the design of two-phase bypass systems in steam turbine plants and of venting valves in the chemical and power industries.

The critical flow rate is the maximum flow rate that can be attained by a compressible fluid as it passes from a high-pressure region to a low-pressure region. Although the flow rate of an incompressible fluid from the high-pressure region can be increased by reducing the receiving end pressure, a compressible fluid flow rate reaches a maximum for a certain (critical) receiving end pressure. This condition occurs for both single flow of gases as well as two-phase gas-liq-

uid flows.

A review of the analytical models and key experimental results of critical two-phase flow shows the following:

1. There are basically three categories of critical two-phase flow models [1]: (1) Analytical models that range from the homogeneous equilibrium model (e.g., Henry and Fauske model) to methods that attempt to account for mechanical (Moody's model) and thermal non-equilibrium phenomena, (2) fitted models such as the RETRAN procedures, and (3) numerical solutions of the conservation equations (e.g., Richter developed a mechanistic non-equilibrium two-fluid model which uses two mass conservation, two momentum conservation, and one mixture energy conservation equations).
2. Although the critical flow of single-phase compressible fluids may be considered as fairly well understood, a complete theory describing the critical flow of two-phase steam-water mixtures is not available yet. Furthermore, comparisons of various critical two-phase flow models with experimental data (for subcooled inlet conditions) obtained by Elias and Lellouche [1] showed that none of the existing analytical models lead to a complete clustering around the equality line within 50 %.
3. The selected critical flow data from the Ilic compilation [2] shows that the ranges of test section diameters (D) and lengths (L) are from 3.2 mm to 76.2 mm and from 0 to 3,700 mm, respectively. Another major source of data, i.e., Marviken data [3] provides very large diameter (from 200 to 509 mm) and pipe lengths from 166 to 1,809 mm. In the Marviken blowdown tests [3], the initial subcooling of the liquid in the vessel varied from 2 to 52 ℃, and the pressure ranged from 4.1 to 5.1 *MPa*. The results showed a strong dependence of the mass flux on the degree of subcooling. The critical flow rate for the subcooled water is higher than that for the saturated water due to the larger fraction of single-phase in the flow.
4. The critical flow rate of a two-phase mixture flowing out of a pressurized vessel is affected by a variety of factors such as the fluid stagnation conditions, the location of flashing inception within a pipe, length to diameter ratio, pipe geometry, fluid properties, and local and frictional pressure losses in the flow channel [1, 4].

As the degree of subcooling (T_{sub}) strongly affects in the determination of critical flow rate (G_c), it is necessary to establish the relationship between two parameters (i.e., T_{sub} versus G_c). However, the range of subcooling covered in the previous experiments is not sufficiently large (i.e., less than 30 ℃) to quantify the effect of subcooling on the critical flow phenomena. Quantification of the relationship between T_{sub} and G_c may help developing a simple critical flow model. In addition, experimental data for small diameters (D less than 10 mm) with short test section lengths (L = 100~400 mm) are extremely rare.

It is the main purpose of this paper to present experimental critical two-phase flow data obtained for wide ranges of subcooling (0~199℃) and pressure (0.5~2.0 MPa) using small diameters (D = 3.4~7.15 mm) with short test section lengths (L = 100~400 mm). In addition, an empirical correlation for critical two-phase mass flux expressed in terms of dimensionless subcooling is presented. This correlation can predict critical two-phase mass flux for wide ranges of stagnation and geometrical conditions.

2. Experimental Methods

A total of 135 critical two-phase flow tests were conducted by discharging high pressure water (0.5~2.0 MPa) from a blowdown vessel to the collection tank maintained at atmospheric pressure through four different test sections as summarized in Table 1. The major thermodynamic and geometric test parameters were the initial subcooling of the water in the vessel and the pipe size (i.e., D, L, and L/D).

Table 1. The Blowdown Test Conditions

Test Section No.	Pressure (MPa)	Subcooling (℃)	Diameter (mm)	Length (mm)	*L/D*	No. of Run
1	0.5	0.3−127.3	3.4	100	29.4	10
	1.0	0.0−158.7				11
	1.5	0.0−181.9				11
	2.0	1.1−191.3				12
2	0.5	0.9−131.5	7.1	100	14.1	9
	1.0	0.0−160.6				10
	1.5	0.5−183.3				10
3	0.5	3.0−140.3	7.15	200	28.0	7
	1.0	1.3−166.3				12
	1.5	2.0−184.2				11
	2.0	0.0−199.3				14
4	1.0	0.7−164.9	7.15	400	55.9	9
	1.5	3.3−184.0				9

2.1. Test Apparatus and Measurement

The schematic of the blowdown apparatus designed to obtain critical two-phase flows in a test section is shown in Fig. 1. Various dimensions of the test section No. 1 and the locations of pressure taps are shown in Fig. 2.

The blowdown test loop consists of the following: (1) a test section, (2) a blowdown vessel equipped with an internal electric heater, (3) an accumulator, (4) a nitrogen tank, (5) a collection tank, (6) associated sensors and devices to measure temperatures, pressures, and water level, and (7) data acquisition systems.

Nitrogen was supplied to the blowdown vessel from the accumulator which is connected to the nitrogen tank. The pressure of the accumulator can be kept at constant value by means of a pressure regulator. During a test, the blowdown vessel is kept at a desired pressure with the pressurized nitrogen. An

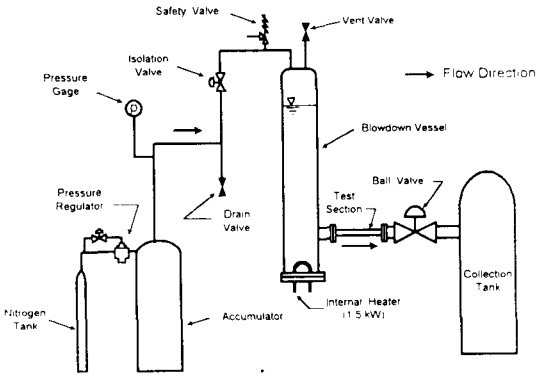

Fig. 1. Schematic Diagram of Blowdown Test Apparatus

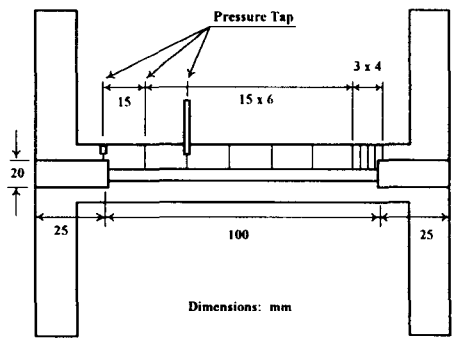

Fig. 2. Static Pressure Measurement in Critical Flow Test Section No. 1 (*D*=3.4 mm, *L*=100 mm)

internal electric heater (1.5 kW) is used to heat the water in the blowdown vessel. In addition, variable capacity external heaters (1.5 kW) are also used to heat the vessel and the test section wall. The mass flux through the test section was determined indirectly via continuous measurements of the water level in the blowdown vessel. The axial pressure distribution along the test section has been obtained from eleven pressure taps which are shown in Fig. 2. In the exit region of the test section, in particular, pressure taps were closer to each other. Also, the pressures and temperatures inside the blowdown vessel as well as at the inlet of the test section and the water level in the blowdown vessel along with the pressures along the test section were continuously recorded at the frequency of 20 samples/sec for each test run.

2.2. Major Test Parameters and Procedures

The major test parameters in the present experiment are the geometry of the test section (i.e., the diameter and the length of the pipe) and the initial subcooling of the water in the blowdown vessel. A particular effort has been made to investigate the critical flow phenomenon for short pipes ($L=100\sim400$ mm) with small diameters ($D=3.4\sim7.15$ mm).

To quantify the effect of subcooling on the critical flow phenomenon, a total of 135 runs were made for a wide range of subcooling of the water at the inlet of the test section using four different L/D test sections as shown in Table 1. The range of blowdown vessel pressures was from 0.5 to 2.0 MPa.

The blowdown vessel was initially filled with de-mineralized water and heated with the internal heater at atmospheric pressure. When the temperature of the water reached a desired value, the blowdown vessel was vented for two to three minutes to remove any dissolved gas in the water. Then the pressure of the accumulator was adjusted to the desired level by means of the pressure regulator. When the pressure of the blowdown vessel reached the initial condition for the test by opening the gas isolation valve, the ball valve located between the exit of the test section and the collection tank (which is open to the atmospheric condition) was then opened to obtain a quasi-steady two-phase flow through the test section. In this manner, a series of experiments have been performed for various combinations of test parameters.

The form and the frictional loss coefficients of the test section for each blowdown vessel pressure were determined from the cold water (~20 ℃) test results for each test section, and these values were used in the determination of the discharge rate for higher temperature conditions.

3. Experimental Results and a Correlation Obtained

3.1. Effects of Various Parameters on Subcooled Critical Two-Phase Flow Rates

3.1.1. Determination of Flashing Inception Location

There is a significant variation in subcooled critical two-phase flow rates through short and long pipes depending on the location of flashing inception within a pipe [4]. The location of flashing inception, on the other hand, strongly depends on the initial subcooling of the water in the blowdown vessel.

In the present work, the location of flashing inception has been determined as depicted in Fig. 3. The approximate region where the flashing can occur has been found by drawing a straight line through a number of measured axial pressure data points that lie upstream of P_{sat} (the saturation pressure corresponding to the liquid stagnation temperature). In Fig. 3, P_{sat} is indicated by a horizontal dashed line. The upstream of the intersection of two straight lines (i.e., point 'C' of Fig. 3) corresponds to the single-phase flow region characterized by a linear pressure drop, whereas the downstream of the point 'C' correspon-

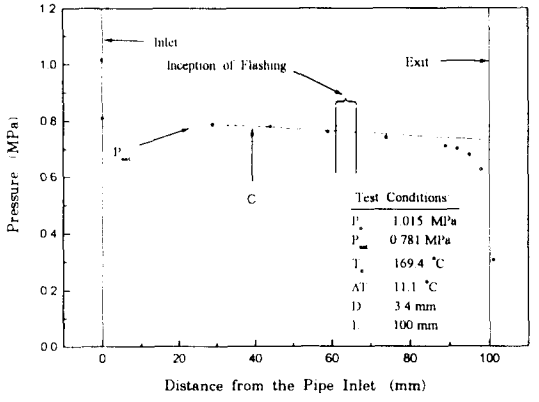

Fig. 3. Measured Pressure Variations and the Location of Flashing Inception within a Pipe for Subcooled Two-Phase Flow Test

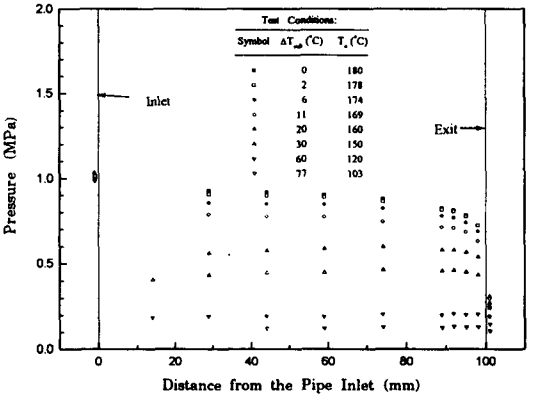

Fig. 4. Measured Pressure Profiles Along the Test Section for Various Initial Subcooling of the Water

ds to the two-phase flow region. The possible region of flashing inception is the region where the pressure drop profile begins to deviate from the solid straight line represented by a bracket in Fig. 3.

3.1.2. Effects of Flashing Inception

The pressure variation measured along the test section No. 1 is plotted in Fig. 4 using the initial subcooling of the water in the blowdown vessel as a major parameter. Following observations can be made in Fig. 4 :

1. As the stagnation subcooling is increased, the location of flashing inception tends to move toward the pipe exit. This result agrees with the work of Fraser and Abdelmessih [4] who concluded that, at highly subcooled stagnation states, flashing inception only occurred near the pipe exit.
2. For higher subcooling ($T_{sub}>20$ ℃), the pressure gradient near the inlet region tends to be slightly positive. However, this phenomenon does not exist at sufficiently low subcooling ($T_{sub}<10$ ℃).

Dimensionless distances from the pipe inlet to the location of saturation pressure (defined by $L^*=L_{sat}/L$) as a function of the dimensionless subcooling (defined by $T^*_{sub}=(T_{sat}-T_o)/(T_{sat}-T_{ref})$ obtained in the present work are shown in Fig. 5 along with

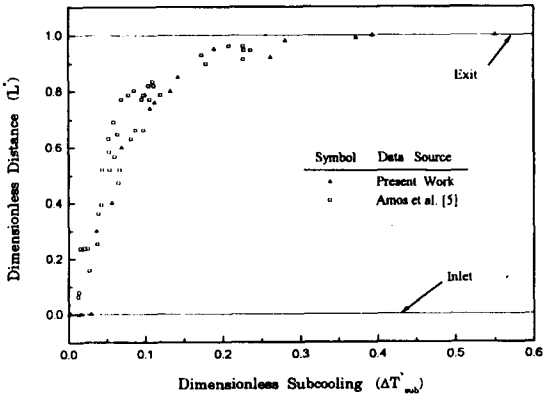

Fig. 5. Dimensionless Distance from the Pipe Inlet to the Location of Saturation Pressure versus Dimensionless Subcooling

the data of Amos and Schrock [5]. This figure shows that the flashing occurs at the exit when T^*_{sub} is greater than about 0.4. This implies that when $T^*_{sub}>0.4$, the critical two-phase flow rate would not noticeably increase by increasing the T^*_{sub} value alone. With regard to this phenomenon, some valuable insight can be gained from the results of Fraser and Abdelmessih [4]. For fixed stagnation conditions, the maximum critical mass flux occurred with flashing inception located near the pipe exit, while minimum critical mass flux occurred with the flashing front located further upstream.

3.1.3. Effects of Stagnation Temperature and Pressure

The mass flux (G) versus the stagnation temperature (T_o) for four different stagnation pressures (P_o) obtained by the present experiment using the test section No. 1 is compared with the predictions of Fauske's equilibrium rate model (ERM) [6] in Fig. 6. From this figure, the following observations can be made:

1. For a given stagnation temperature, the mass flux increases as the stagnation pressure is increased as can be expected.
2. For a fixed stagnation pressure, the rate of decrease of the mass flux becomes larger as the stagnation temperature is increased.
3. The ERM of Fauske [6] also predicts similar trends noted above. However, this model tends to over-predict the mass flux for higher subcooling regions, in particular, whereas the agreement between the model predictions and the data becomes relatively better for lower subcooling regions. This result is expected since the ERM has been developed for the case of insignificant frictional loss. For the higher subcooling regions, the ERM overpredicts the flow rate, since the flow limitation caused by the friction force for higher mass flow condition is significant.

3.1.4. Effects of Pipe Size

To examine the effects of pipe size (i.e., D, L, and L/D) on subcooled critical two-phase flow rates, the measured mass fluxes through four different test sections (L/D=14.1~55.9; D=3.4~7.15 mm; L=100~400 mm) are plotted against the stagnation temperature in Fig.7. This figure shows the following:

1. Results of test sections No. 1 (D=3.4 mm; L=100 mm) and No. 2 (D=7.1 mm; L=100 mm) clearly show that the mass flux of the larger pipe diameter is greater for the same pipe length and stagnation temperature conditions.
2. Results of test sections No. 3 (D=7.15 mm; L=200 mm) and No. 4 (D=7.15 mm; L=400 mm) show that when the pipe diameter and the stagnation temperature are the same, the mass flux from a longer pipe is smaller than that from a shorter pipe.
3. A comparison between the results of test sections No. 1 and No. 3 shows that the mass flux of the shorter pipe (i.e., test section No. 1) is larger than that of the longer pipe for a given stagnation temperature when L/D is about the same.

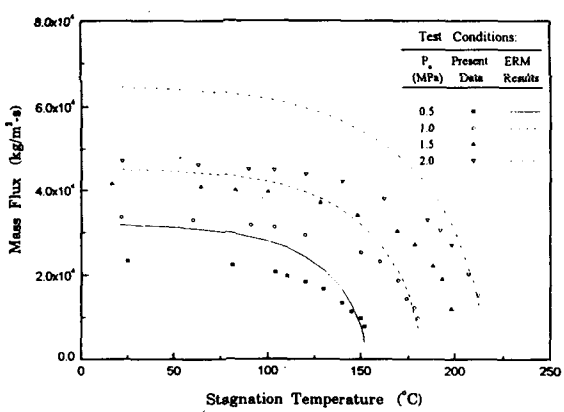

Fig. 6. Mass Flux Versus Stagnation Temperature for Four Different Stagnation Pressures Obtained by Present Experiment and Equilibrium Rate Model (ERM) of Fauske

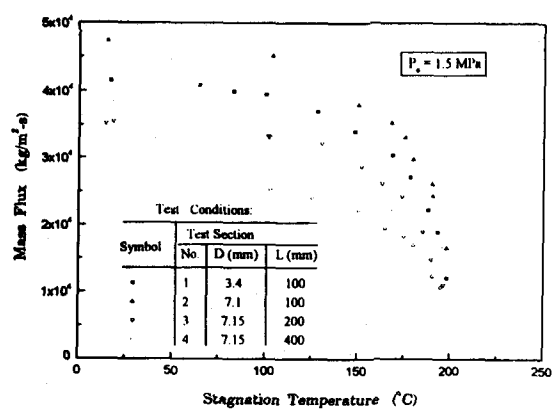

Fig. 7. Effects of Tube Size on Subcooled Critical Two-Phase Flow Rates

3.2. Derivation of an Empirical Correlation

In an effort to find an appropriate functional relationship between the critical two-phase mass flux (G_c) and the stagnation temperature (T_o) that does not depend on the pipe size (D, L, and L/D), two dimensionless numbers are defined based on the insights gained from the analysis of the present experimental data. Two dimensionless numbers defined here are (1) the dimensionless mass flux (G^*) and (2) the dimensionless subcooling (T^*_{sub}). They are defined as follows :

$$G^* \equiv \frac{G_c}{G_{ref}} \tag{1}$$

where

$$G_{ref} \equiv \left[\frac{2\rho(P_o - P_b)}{1 + K + f\frac{L}{D}}\right]_{ref}^{0.5} \tag{2}$$

and

$$\Delta T^*_{sub} \equiv \frac{T_{sat} - T_o}{T_{sat} - T_{ref}} \tag{3}$$

G_{ref} and the denominator in Eq. (2) are the mass flux for cold water and the discharge coefficient evaluated at the reference temperature (i.e., $T_{ref}=20$℃) and the stagnation pressure (P_o), respectively.

The G^* versus T^*_{sub} for all the experimental data obtained from four different test sections (No. 1~No. 4) are plotted in Fig. 8. This figure strongly suggests that all the G^* versus T^*_{sub} data obtained from all four different test sections can be represented by a single expression. Therefore, applying a nonlinear least squares curve fitting procedure to the G^* versus T^*_{sub} data shown in Fig. 8, the following expression for G^* has been obtained in terms of T^*_{sub} :

$$G^* = 1 - \frac{15.2}{1 + \exp[(\Delta T^*_{sub} + 0.578)/0.188]} \tag{4}$$

Combining Eqs. (1) and (4), the final empirical correlation for subcooled two-phase flow rates through short pipes with small diameters is obtained as follows :

$$G_c = \left[\frac{2\rho(P_o - P_b)}{1 + K + f\frac{L}{D}}\right]_{ref}^{0.5} \left\{1 - \frac{15.2}{1 + \exp[(\Delta T^*_{sub} + 0.578)/0.188]}\right\} \tag{5}$$

The above Eq. (5) can be rewritten as :

$$G_c = (C_d)_{ref}\left[2\rho(P_o - P_b)\right]_{ref}^{0.5} \left\{1 - \frac{15.2}{1 + \exp[(\Delta T^*_{sub} + 0.578)/0.188]}\right\} \tag{6}$$

where

$$(C_d)_{ref} = \left(1 + K + f\frac{L}{D}\right)_{ref}^{-0.5} \tag{7}$$

For given flow conditions (i.e., flow geometry, stagnation conditions, and receiving end pressure), the critical two-phase flow rates of subcooled water through short pipes (L=100~400 mm) with small diameters (D=3.4~7.15 mm) can be calculated from Eq. (5) or Eq. (6) when the mass flux of water at 20 ℃ (G_{ref}) defined by Eq. (2) or the discharge coefficient for water at 20 ℃, $(C_d)_{ref}$, given by Eq. (7) is

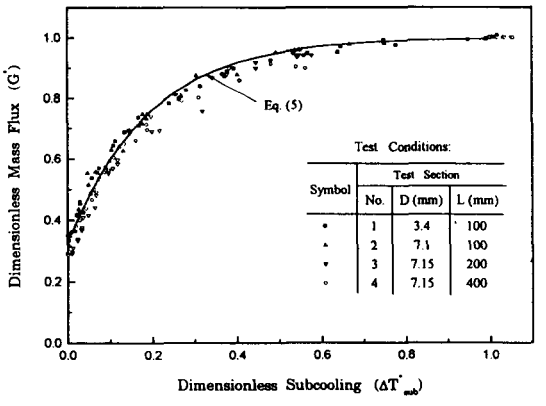

Fig. 8. Dimensionless Mass Flux Versus Dimensionless Subcooling for Four Different Size Tubes

available or can be calculated.

4. Comparison Between Experimental Data and Correlation

The selected critical flow data for comparison with the present correlation are summarized in Table 2. These experiments comprise 755 data points with pressures from 0.21 to 17.0 MPa, diameters from 0.25 to 509 mm and lengths from approximately zero to 2,335 mm. These data are from 9 different experimenters that include both for horizontal and vertical flows.

To compare the data shown in Table 2 with predictions of present correlation, G_{ref} or $(C_d)_{ref}$ value should be calculated first. For those data points where K and f values are available (e.g., Amos et al. and John et al.'s data), $(C_d)_{ref}$ has been calculated using Eq. (7). However, when neither K and f nor G_{ref} values are obtainable for given data set, G_{ref} value for the lowest temperature case (i.e., the most highly subcooled data point) has been calculated from Eqs. (1) and (4) and this value is used for the rest of the data points at higher temperatures.

A comparison of critical mass fluxes calculated by present correlation, Eq. (5), and a total of 755 selected experimental data points from 9 different sources is given in Fig. 9. Considering the fact that these experimental data are from a wide range of test section sizes, geometries, flow orientations, and stagnation conditions as can be seen in Table 2, the agreement is generally good except for low subcooling data obtained from orifices with small L/D (i.e., less than 10).

Also, the statistical indicators estimated to examine the agreement between the present empirical correlation with data, i.e., the mean relative difference between the data and the calculated values ($\bar{X}$) and

Table 2. Selected Critical Flow Data and Comparison with the Present Model

Experiment	Pressure (MPa)	Hydraulic Diameter (mm)	Flow Length (mm)	No. of Data	$\bar{X}$ (%)	σ (%)	Remarks
Amos et al. [5]	4.1-16.2	0.25-0.76	63.5	72	−4.4	10.4	Slit Down Flow
John et al. [7]	4.0-14.0	0.41-1.28	46.0	57	2.5	9.9	Slit Down Flow
Celata et al. [8]	0.8-2.3	4.6	46-1380	60	−3.2	6.0	Pipe Down Flow
Jeandey et al. [9]	2.0-12.0	20.13	363	88	−2.4	6.8	Pipe Up Flow
Sozzi et al. [10]	3.0-7.0	12.7	0-1778	210	−0.2	11.0	Transient, Pipe, Nozzle Horizontal
Reocreux [11]	0.21-0.34	20	2335	39	−3.6	6.8	Pipe Up Flow
Powell [12]	4.2-17.0	11.1	–	41	3.3	7.3	Converging-Diverging Nozzle
Marviken [3]	4.0-5.0	200-509	166-1589	53	1.4	5.2	Transient Pipe, Down Flow
Present Work	0.5-2.0	3.4-7.15	100-400	135	−2.8	6.3	Pipe, Horizontal
	Total			755	−1.2	8.9	

the standard deviation (σ) are given in Table 2. Here $\bar{X}$ and σ are defined by the following equations :

$$\sigma = \left(\sum_{i=1}^{n} \frac{(X_i - \bar{X})^2}{n-1} \right)^{0.5} \quad (8)$$

where

$$\bar{X} = \frac{1}{n} \sum_{i=1}^{n} X_i \quad (9)$$

and

$$X_i = \left(\frac{G_{exp} - G_{corr}}{G_{exp}} \right)_i \times 100 \ \% \quad (10)$$

where n is the number of data.

5. Conclusions

Critical two-phase flow rates of subcooled water through short pipes with small diameters have been experimentally investigated for wide ranges of subcooling and pressure. To examine the effects of various parameters on the critical two-phase flow rates of subcooled water through present test sections, a total of 135 runs were made for various combinations of test parameters using four different L/D test sections.

Experimental results that show effects of various parameters on subcooled critical two-phase flow rates are presented in graphical forms such as the dimensionless mass flux versus the dimensionless subcooling curve. In addition, an empirical correlation for subcooled two-phase flow rates through present test sections has been obtained in terms of a dimensionless subcooling (T^*_{sub}). A comparison of critical mass fluxes calculated by the present correlation and a total of 755 selected experimental data points from 9 different experimenters shows that the agreement is generally good except for very low subcooling data obtained from orifices with small L/D (less than 10).

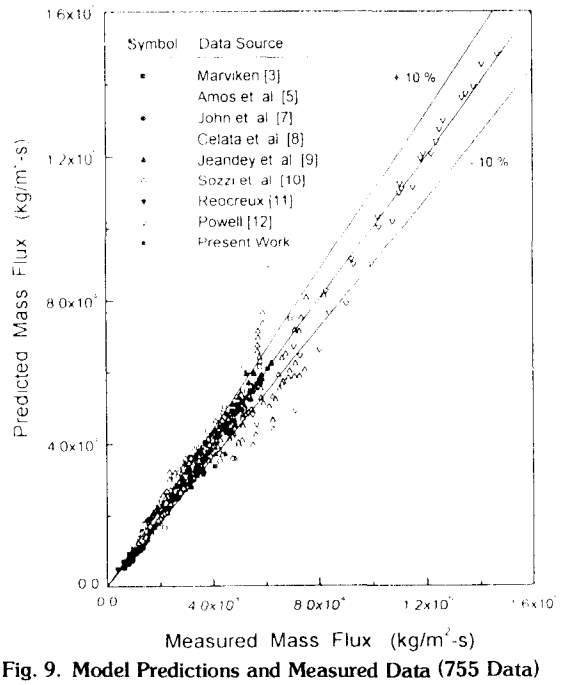

Fig. 9. Model Predictions and Measured Data (755 Data)

Nomenclature

$(C_d)_{ref}$	discharge coefficient evaluated at 20℃
D	diameter, mm
f	friction factor
G	mass flux, kg/m^{2}s
G^*	dimensionless mass flux, G_c/G_{ref}
G_c	critical mass flux, kg/m^{2}s
G_{corr}	critical mass flux calculated by Eq. (5), kg/m^{2}s
G_{exp}	critical mass flux obtained by experiment, kg/m^{2}s
G_{ref}	mass flux of water at 20 ℃, kg/m^{2}s
i	index
K	pipe entrance loss coefficient
L	pipe length, mm
L^*	dimensionless distance, L_{sat}/L
L_{sat}	distance from the pipe inlet to the location of saturation pressure, mm
n	number of data
P	pressure, MPa
P_b	back pressure, MPa
P_o	stagnation pressure, MPa
P_{sat}	saturation pressure corresponding to T_o, MPa
T	temperature, ℃
T_o	stagnation temperature, ℃

T_{ref} reference temperature, 20 ℃
T_{sat} saturation temperature corresponding to P_o, ℃
T_{sub} subcooling, ℃
T^*_{sub} dimensionless subcooling, $(T_{sat}-T_o)/(T_{sat}-T_{ref})$
$\overline{X}$ mean relative difference between mass flux measured by experiment and those calculated by present correlation, %
X_i i-th fractional error defined by Eq. (9), %
ρ density of water, kg/m^3
σ standard deviation, %

Subscript

b receiver system
c critical
corr correlation
exp experiment
o stagnation condition
ref values at 20 ℃
sat saturation condition

Superscript

* dimensionless
− mean value

References

1. E. Elias and G. S. Lellouche, "Two-Phase Critical Flow," Int. J. Multi-phase Flow, Vol. 20, Suppl., pp. 91-168 (1994)
2. V. Ilic, S. Banerjee, and S. Behling, "A Qualified Database for the Critical Flow of Water," EPRI NP-4556 (1986)
3. "The Marviken Full-Scale Critical Flow Tests," NUREG/CR-2671, MXC-301 (1982)
4. D.W.H. Fraser and A.H. Abdelmessih, "A Generalized Unified Non-Equilibrium Model for Predicting Saturated and Subcooled Critical Two-Phase Flow Rates Through Short and Long Tubes," Proceeding of the 7th International Meeting on Nuclear Reactor Thermal Hydraulics, NURETH-7, Held at Sheraton Hotel & Convention Center, Saratoga Springs, New York, NUREG/CP-0142, Vol. 3, pp. 264-283, Sep. 10-15 (1995)
5. C.N. Amos and V.E. Schrock, "Critical Discharge of Initially Subcooled Water Through Slits," NUREG/CR-3475 (1983)
6. H.K. Fauske, "Flashing Flows or : Some Practical Guidelines for Emergency Releases," Plant/Operations Progress, Vol. 4, No. 3, pp. 132-134 (1985)
7. H. John et al., "Critical Two-Phase Flow through Rough Slits," Int. J. Multiphase Flow, Vol. 14, No. 2, pp. 155-174 (1988)
8. G.P. Celata et al., "Two-Phase Flow Models in Unbounded Two-Phase Critical Flows," Nuclear Engineering and Design, Vol. 97, pp. 211-222 (1986)
9. C. Jeandey et al., "Auto Vaporization d'Ecoulements Eau/Vapeur," CEN de Grenoble, Report T.T. No. 163 (1981)
10. G.L. Sozzi and W.A. Sutherland, "Critical Flow of Saturated and Subcooled Water at High Pressure," NEDO-13418 (1975)
11. M. Reocreux, "A Contribution a l'Etude des Debits Critiques en Recoulement Diphasique Eau/Vapeur," Doctoral Dissertation a l'Universite Scientifique et Medicale de Grenoble (1974)
12. A. W. Powell, "Flow of Subcooled Water Through Nozzles," WAPD-PT(V)-90 (1961)